PETROPHYSICS, VOL. 53, NO. 5 (OCTOBER 2012); PAGE 315–331; 28 FIGURES; 2 TABLES

# Hysteresis of Capillary Pressure, Resistivity Index and Relative Permeability in Different Carbonate Rock Types[1]

**Moustafa R. Dernaika[2], Mohammed Z. Kalam[3], Mahmoud A. Basioni[3], Svein M. Skjæveland[4]**


## ABSTRACT

Experimental measurements of capillary pressure, resistivity index and relative permeability display hysteresis manifested through the dependence of these properties on the saturation path and saturation history whenever fluid saturations undergo cyclic processes. At the pore scale, hysteresis is typically influenced by contact-angle hysteresis, trapping of one phase by another and wettability changes.

A laboratory study was conducted to investigate hysteresis effects measured on reservoir core plugs for a major carbonate hydrocarbon reservoir in the Middle East. Representative core samples covering reservoir rock types (RRT) were selected based on whole-core and plug X-ray CT, high-pressure mercury injection, porosity, permeability and thin-section analyses.

Primary drainage and imbibition capillary pressure and resistivity index (*PcRI*) were measured by the porous-plate method using stock tank oil and simulated formation brine at reservoir temperature and overburden conditions. Large hysteresis effects were obtained between primary drainage and imbibition for both $P_c$ and *RI* curves. Low residual oil saturations ($S_{or}$) were measured at the end of forced imbibition indicating oil-wet to mixed-wet characteristics. Nonlinear *RI* curves were found during imbibition which could not be described by conventional Archie equation. Water-oil relative permeability curves were measured on similar reservoir core samples by the steady-state technique using live fluids at full reservoir conditions with in-situ saturation monitoring. Hysteresis effects on both oil and water curves were observed between primary drainage and imbibition, and appear to be influenced by the sample rock type involved (i.e. wettability and pore structure).

The strong hysteresis in *RI* was explained by a fluid invasion behavior at the pore level, and was attributed to varying displacement mechanisms between primary drainage and imbibition. Conventional assumption of Archie behavior is therefore not always valid for such carbonate rock types. This *RI* hysteresis, together with the variation of $K_r$ hysteresis trends with different rock types, may help improve the current hysteresis models and provide better understanding of the hysteresis phenomena in natural porous media.


## INTRODUCTION

Knowledge of hysteresis phenomena in porous media is necessary for the understanding of saturation distributions in complicated reservoir flow histories and in many EOR applications (Jerauld and Slater, 1990).

Fleury et al. (2004) reported strong hysteresis in resistivity index (*RI*) between primary drainage and imbibition, which had large impact on log data calibration. The behavior was referred to the strong hysteresis in capillary-pressure curves but detailed understanding or description of the mechanism involved was still lacking. The hysteresis data were obtained using the fast resistivity-index measurement (FRIM) method.

Masalmeh (2001) presented a conceptual hysteresis model that attributed hysteresis to three main factors: fluid trapping, contact angle hysteresis and wettability changes. The model explained most of the observed trends in capillary-pressure ($P_c$) and relative-permeability ($K_r$) hysteresis. Schematic diagrams of the relative-permeability hysteresis between primary drainage and imbibition on both oil and water curves are presented for water-wet and oil-wet cases in Figs. 1 and 2, respectively. We choose to present this $K_r$ hysteresis model schematically due to the scarcity of such experimental curves and because it relates to our experimental data presented in this paper. Figures 1 and 2 show respectively the $K_r$ hysteresis trends

Manuscript received by the Editor October 3, 2011; revised manuscript received October 9, 2012.
[1]Originally presented at the International Symposium of the Society of Core Analysts, Austin, TX, USA, September 18–21, 2011, Paper SCA2011-14.
[2]Ingrain Inc., P.O. Box 114568, Ascent Business Centre, Building No. 4, Mussafah 12, Abu Dhabi, U.A.E; Email: dernaika@ingrainrocks.com
[3]ADCO, Abu Dhabi Company for Onshore Oil Operations, P.O. Box 270, Abu Dhabi, U.A.E; Email: mkalam@adco.ae, mbasioni@adco.ae
[4]The University of Stavanger, 4036 Stavanger, Norway; Email: s-skj@ux.uis.no

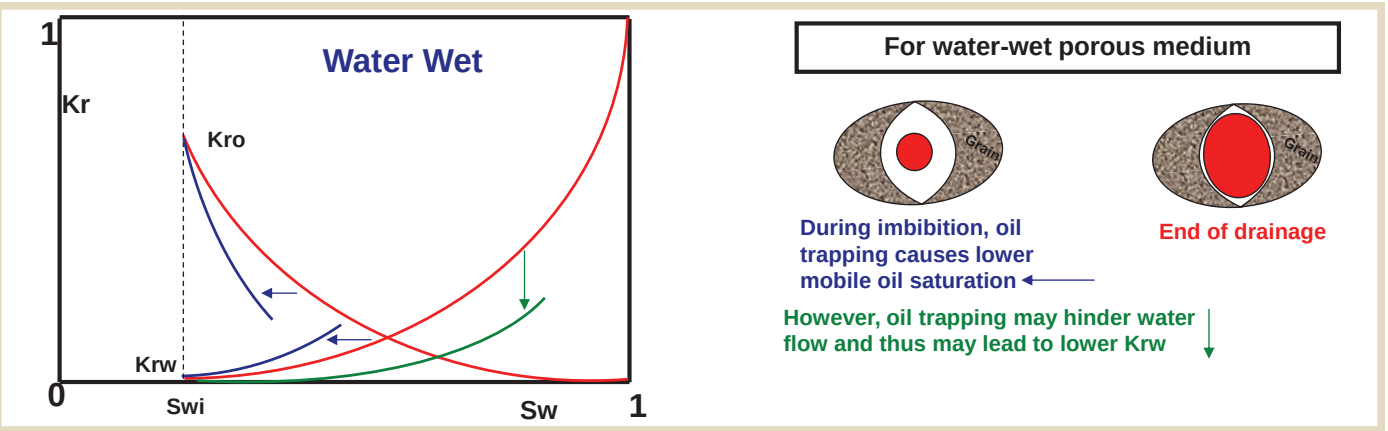


**Fig. 1**–Schematic diagram for water-wet $K_r$ hysteresis based on conceptual model (Maselmeh, 2001).

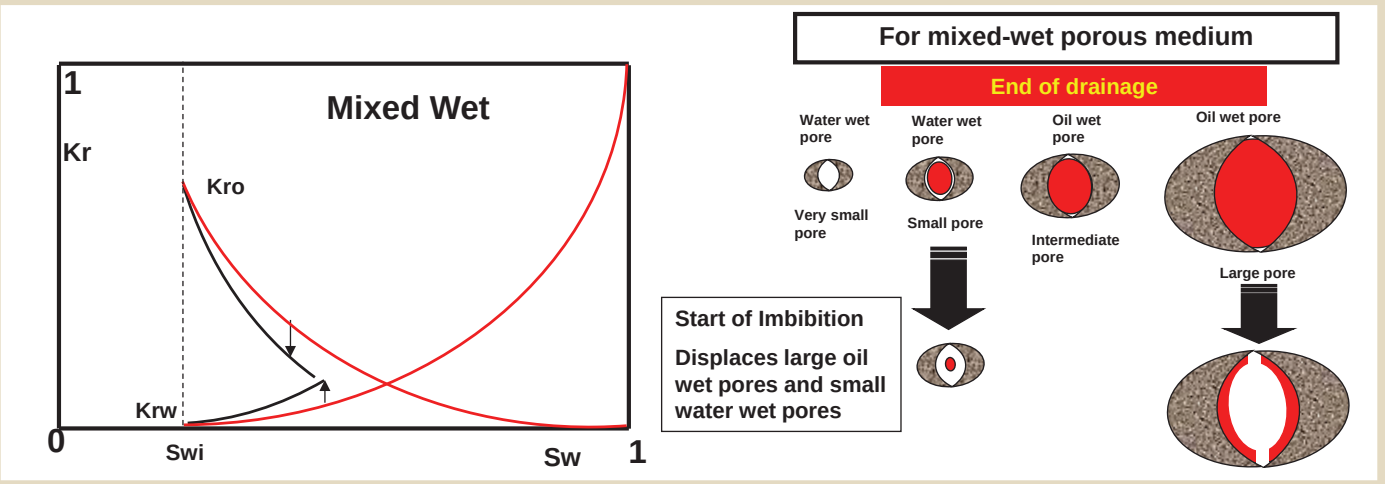


**Fig. 2**–Schematic diagram for mixed-wet $K_r$ hysteresis based on conceptual model (Maselmeh, 2001).

for water-wet and oil-wet scenarios with brief explanations of the fluid-flow mechanisms and sequence of invasion. For the water-wet case both imbibition relative permeability to oil ($K_{ro}$) and to water ($K_{rw}$) are shifted to lower water saturations due to oil trapping, which causes lower mobile oil saturation. This will cause the imbibition $K_{ro}$ to be lower than the primary drainage $K_{ro}$ curve, and will cause the imbibition $K_{rw}$ to be higher than the primary drainage $K_{rw}$. However, oil trapping may hinder water flow and thus may lead to lower imbibition $K_{rw}$ than the primary drainage $K_{rw}$. Hence, there will be two opposing effects on the imbibition $K_{rw}$ and, which in many cases can cause no major hysteresis in the $K_{rw}$ curve between primary drainage and imbibition in water wet systems. For the mixed-wet case, imbibition will start displacing big oil-wet pores and small water-wet pores. Water will occupy more large pores during imbibition than during primary drainage, and this may lead to higher imbibition $K_{rw}$ than primary drainage $K_{rw}$ curve. Imbibition $K_{ro}$ will be lower than the primary drainage $K_{ro}$ since there will be fewer large pores occupied with oil. This is only a brief introduction to the relative permeability conceptual hysteresis model between primary drainage and imbibition. More details can be found in Masalmeh (2001).

In this paper we present experimental hysteresis in capillary pressure, resistivity index and relative permeability between primary drainage and imbibition on different carbonate rock types. The rock types were initially characterized by static rock typing which is based on petrophysical data and geological description. The static rock characterization does not include imbibition dynamic data. Static rock typing is important for initializing reservoir static models while imbibition data are essential in modeling secondary and tertiary recovery processes. The established reservoir rock types by static data should always be checked when assigning saturation functions ($P_c$ and $K_r$) in dynamic reservoir modeling, and hence one of the objectives in this paper is to evaluate the validity of the static rock types by imbibition relative permeability and hysteresis trends obtained on the different rock types studied in this research work.

The hysteresis in resistivity index and capillary pressure were measured using the porous-plate method, which is known to be a very reliable technique, where both the $P_c$ and $RI$ data are obtained simultaneously. These data are not available in the literature for different carbonate rock types at reservoir conditions. The reason for this is probably

due to the prolonged times it takes to conduct porous-plate experiments with equilibrium capillary-pressure steps. The hysteresis of the relative permeability in this work was studied between primary drainage and imbibition using the steady-state technique. The experiments were performed at full reservoir conditions using live fluids, and the saturations were monitored by in-situ saturation profiles using gamma ray. These experiments were used to study the effect of different carbonate rock types on the experimental hysteresis trends. Such data are rather scarce in the literature as most of the available data are either measured on water-wet rocks or on limited rock types. The hysteresis data provided in this work are needed to enrich the available hysteresis models that may lack a complete and consistent description of the hysteresis phenomena in porous media. In the experimental data of this work, strong hysteresis was found in resistivity index and capillary-pressure curves. We suggest a pore-level scenario for the fluid flow and distribution to explain the resistivity index hysteresis, which was lacking in previous publications. Relative permeability hysteresis showed different patterns for different rock types which could possibly be attributed to the complex relation between the effects of wettability and pore structure.

Throughout this paper drainage is used to describe oil displacing water. Imbibition describes water displacing oil regardless of wettability condition. Primary drainage is used to represent oil displacing water from 100% water saturation. Spontaneous imbibition refers to water displacing oil in water-wet pores, and forced imbibition is used to refer to imbibition in mixed-wet pores. For convenience, we will sometimes use the term "oil wet" to refer to "mixed wet."

## HYSTERESIS

Hysteresis refers to irreversibility or path dependence. For saturation-dependent rock properties such as capillary pressure, resistivity index and relative permeability, hysteresis manifests itself through the dependence of these properties on the saturation path and saturation history. Saturation path refers to flow in drainage or imbibition cycles, while saturation history is a broader term and may also refer to saturation distribution state caused by wettability changes for instance. Hysteresis is primarily caused by contact-angle hysteresis, fluid trapping and wettability (Jerauld and Salter, 1990; Masalmeh, 2001).

Contact-angle hysteresis is the variation in contact angle with the direction of displacement. Water-receding contact angle in drainage is always smaller than water-advancing contact angle in imbibition. This hysteresis is usually attributed to nonequilibrium effects, contamination or heterogeneity of the surface due to either roughness or composition.

Fluid trapping is a result of pore-space geometry and is caused by instabilities in the fluid-fluid interface configurations. Such an instable configuration occurs if an advancing interface undergoes a decrease in curvature in a drainage process. The unstable interface jumps very rapidly displacing wetting phase from the pore. These jumps are known as Haines jumps and are irreversible, and thus cause permanent hysteresis between drainage and imbibition (Melrose, 1965). Haines jumps may be pronounced, with large aspect ratios (pore body to pore throat), which in turn have a direct effect on hysteresis loops (Toledo et al., 1994).

Wettability is the overall tendency of a reservoir rock to prefer one fluid over another (Longeron et al., 1994), and has been recognized as an important factor in remaining oil saturation, and capillary-pressure and relative-permeability curves (Anderson, 1987a, 1987b). It depends on rock pore-size distribution and rock-fluid interactions. It is influenced by fluid composition, rock-surface mineralogy, temperature, pressure and thickness of water films. Upon oil invasion by capillary action a thin film of water remains adsorbed on the pore surface and protects the solid from the oil. When capillary pressure becomes higher, at a certain critical capillary-pressure level, the water film ruptures and oil gets access to the surface. Stability of the water film depends on prevailing capillary pressure and disjoining pressure isotherm (Hirasaki, 1991). The disjoining pressure isotherm is dependent on the surface mineralogy, fluid composition and pore shape. When oil gets in contact with the surface wettability alteration occurs and the degree of alteration will depend on the fluid and surface compositions (i.e. rock-fluid interactions). The pore corners and crevices where water is still present remain water-wet. This leads to development of heterogeneous forms of wettability, where some parts of the rock surface are altered oil-wet, while other parts remain water-wet (Kovscek et al., 1993).

Wettability changes (i.e. absence of thin films) can give rise to considerable hysteresis in the oil-water contact angle (Melrose, 1965). Wettability alteration and contact angle hysteresis have their origins at the microscale. Fluid trapping occurs at a larger scale and is caused by pore morphology. Both wettability changes and hysteresis in contact angle largely affect the degree of trapping.

## DISPLACEMENT MECHANISMS

In primary drainage, oil invasion occurs by piston-like displacement, where oil enters the pore from one of the ends, displacing water originally present. This displacement occurs when the capillary pressure is increased to the capillary entry pressure required for invasion of the interface.

In imbibition, piston-like invasion and snap-off mechanisms are possible. Piston-like invasion occurs when the capillary pressure is decreased to the capillary entry pressure required for the displacement. The capillary entry pressures for both drainage and imbibition are governed by the Laplace equation. Snap-off occurs as a result of increased water content from the corners or by swelling of films in water wet pores. Water may invade the entire cross section and cut off oil, resulting in trapped oil. The amount of trapped oil is strongly dependent on the shape of the

fluid interface. The interface shape is a function of the contact angle and the geometry of the pore. Breakage of the continuity of the oil phase occurs at the junction of the pore with the exit throat. This capillary instability in the exit throat is caused by the interface moving to maintain equal curvature at all points. Snap-off and trapping in single pores appear to be a function of aspect ratio which is defined as pore-throat diameter ratio (Wardlaw, 1982). Snap-off only occurs if piston-like invasion is topologically impossible since the capillary pressure for piston-like invasion is favorable compared to the capillary pressure for snap-off (Lenormand et al., 1983).

Snap-off can be more favorable over piston-like displacement in spontaneous imbibition if the pore is surrounded by several oil-filled throats, when advancing contact angle is small and when the pore system is characterized by large aspect ratio. Hence, the type of pore-level displacement that occurs depends upon whether the process is drainage or imbibition, and the geometry of the pore space.

## EFFECT OF ROCK TYPE ON HYSTERESIS

In this paper, a reservoir rock type (RRT) is initially established based on combined petrophysical properties and geological description. The petrophysical properties used for rock-type classification are porosity, permeability, and mercury-derived drainage capillary pressure ($P_c$) and pore-throat size distribution (PSD). In this paper geological description refers to thin-section analysis, which aims at defining pore systems, facies and depositional environment.

Mercury-derived $P_c$ and PSD curves are widely used in the oil and gas industry, and usually yield accurate results if proper protocols are applied (Masalmeh and Jing, 2006; Serag El Din et al., 2010). Such data are frequently used to provide fast, efficient and cost effective RRT classification. Mercury is used primarily because of its high interfacial tension (485 mN/m) and high contact angle (140° measured through mercury) which make mercury almost spherical in shape. When mercury invades a porous medium it is then possible to calculate the pore-throat radius of the sample in terms of the bundle of capillary-tube model by using the pressure drop across a spherical interface (Laplace equation). It has to be noted in this perspective that mercury intrusion data do not provide direct information about pore diameters, rather they assign the pore-body volumes to their entry throats. Therefore, mercury data contain valuable information about reservoir rocks and rock type because the resistance offered by the pore structure to many transport phenomena is controlled by the pore throats, the sizes of which are derived from the mercury-intrusion data.

Longeron et al. (1989) compared resistivity index data in water wet samples from sandstone and carbonate reservoirs. Their measurements indicated that the resistivity/water-saturation law depended on the microscopic distribution of fluids, hence on the direction of the saturation change (drainage or imbibition) and on the nature of the fluids (water/oil or water/gas).

Dernaika et al. (2007) reported distinct hysteresis patterns between primary drainage and imbibition for capillary-pressure and resistivity-index curves obtained on different carbonate rock types. The distinct hysteresis trends were obtained on samples treated with same fluids (dead crude oil/brine) and performed at the same experimental reservoir conditions. The different hysteresis was attributed to the combined effect of pore geometry and rock-fluid interactions.

Jerauld and Salter (1990) conducted a pore-level modeling study to understand the impact of pore structure on hysteresis behavior in relative permeability and capillary pressure in strongly-wetting systems at low capillary number. They found that the pore-body to pore-throat aspect ratio was the most important structural determinant of the hysteresis behavior. The pore-size distribution was of secondary importance.

These studies together with the underlying pore scale physics clearly demonstrate the role of rock type in yielding various displacement mechanisms that can cause different hysteresis trends in capillary pressure and relative permeability. Different rock types can have different pore geometries including differences in the types of pores, their relative presence and distribution. These differences can cause variations in contact angles, topological fluid-trapping conditions and wettability changes. These variations in rock types can have a direct effect on the displacement mechanism at the pore scale and thus yield variations in hysteresis trends.

## EXPERIMENTAL MEASUREMENTS

### Rock Characterization and Sample Selection

Representative (1.5–in. diameter) core samples were selected from a carbonate field based on whole-core and plug X-ray CT, high-pressure mercury injection, porosity, permeability and thin-section analyses. Seven samples covering the main rock types were selected for capillary-pressure and resistivity-index (*PcRI*) measurements and four samples from high-quality and low-quality rock types were selected for steady-state relative permeability ($K_r$). The best high-permeability rock-type samples were absent in the capillary-pressure and resistivity-index measurements (Fig. 3).

Helium (He) porosity of the selected samples ranged from 16 to 26% and the permeability varied from 0.63 to 46 md (Fig. 3). Pore-throat size distribution (PSD) curves of the selected samples are given in Fig. 4, and thin-section photomicrographs for the good-quality and poor-quality rock types (corresponding to the $K_r$ samples) are shown in Figs. 5 and 6, respectively.

Plug imaging for the $K_r$ samples was done at two different resolutions. First, the plugs were imaged at two energy levels using a customized dual-energy medical

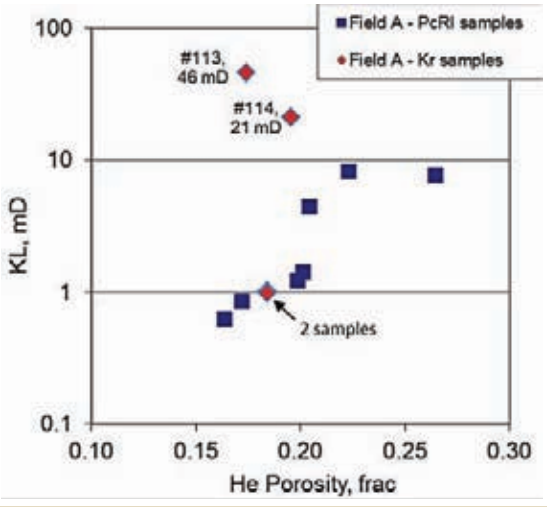


**Fig. 3**–Poroperm for *PcRI* and $K_r$ samples.

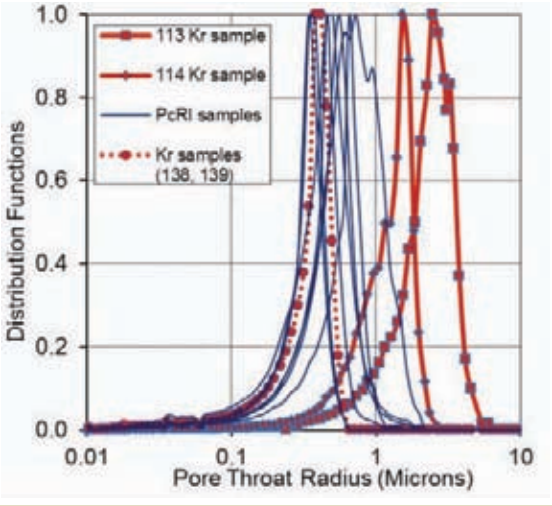


**Fig. 4**–Hg-derived PSD corresponding to Fig. 3.

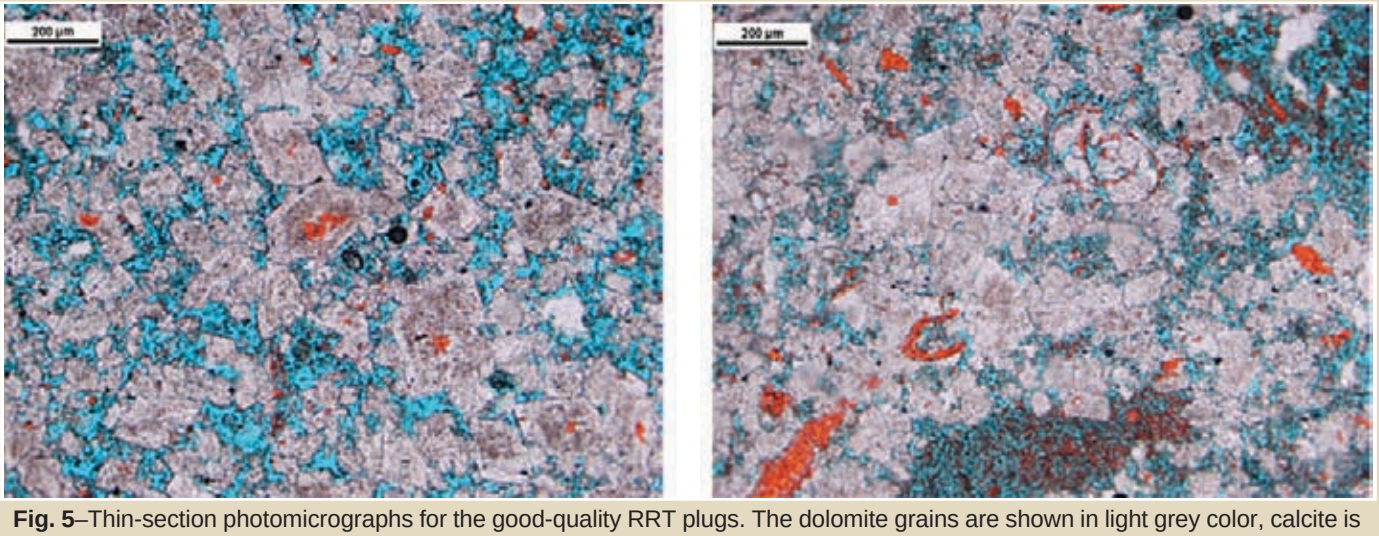


**Fig. 5**–Thin-section photomicrographs for the good-quality RRT plugs. The dolomite grains are shown in light grey color, calcite is represented in red, and the pores in blue.

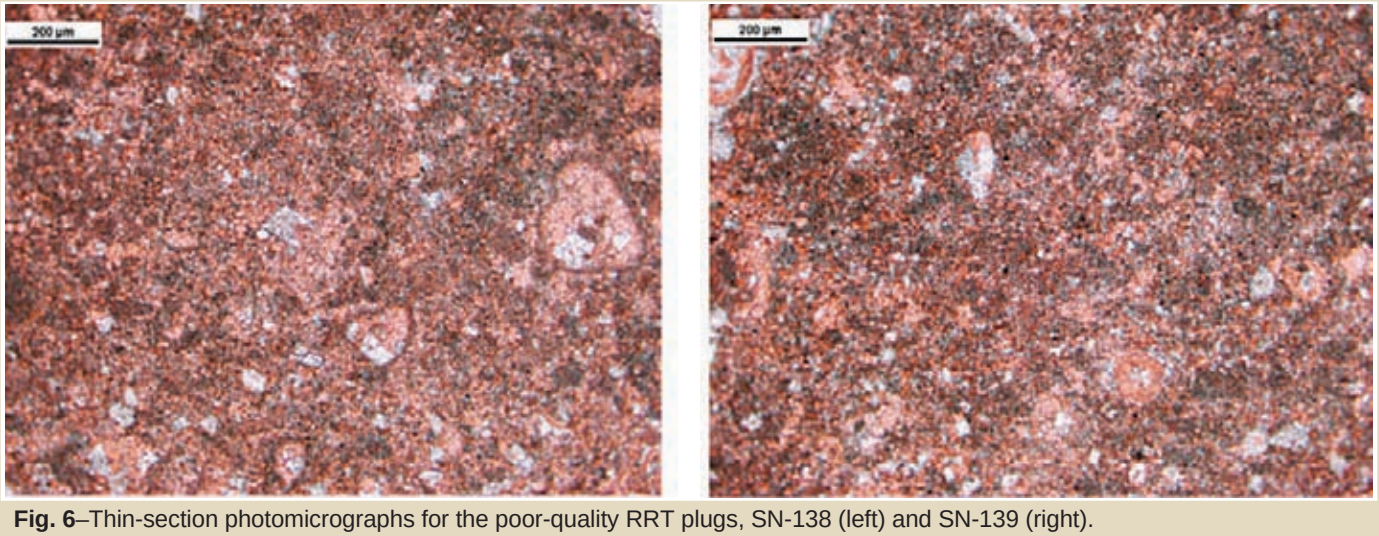


**Fig. 6**–Thin-section photomicrographs for the poor-quality RRT plugs, SN-138 (left) and SN-139 (right).

CT scanner. The images were acquired in helical high-resolution scanning mode and have an in-plane (X-Y) pixel resolution of 352 μm and slice thickness (Z) of 500 μm. Those images are represented in gray scale and color scale, as shown in Figs. 7 and 8. Figure 7 presents the good-quality RRT SN-114 and Fig. 8 presents the poor-quality RRT SN-139. The CT images from plug SN-113 and SN-138 are not presented here but they show similar features to samples SN-114 and SN-139, respectively. The scanning was performed in 3D and the figures show only one of the middle longitudinal slices from each plug sample. Second, the plugs were imaged in a micro-CT scanner with focused X-rays at a resolution of 40 μm per pixel. This is one of the best resolutions that can be acquired on 1.5–in. diameter core plugs, and clearly shows the improvement in the image resolution over the medical scanner. Those images are represented in Figs. 7c and 8c for SN-114 and SN-139, respectively. The same range of pixels is used in the color-scale bar in Figs. 7b and 8b, which allows direct comparison between the different RRT samples. The pixel values in a CT image are influenced by the densities and effective atomic numbers of the rock aggregates. Low pixel values may indicate low density and high porosity, as opposed to high pixel values, which may indicate high density and low porosity values. Direct comparison between the figures shows that the good-quality RRT sample is more heterogeneous with high fraction of low pixels. The distribution of the low-pixel space may be due to the high-permeability channel that shows up as an increase in permeability over the more homogeneous SN-139. The micro-CT images in Figs. 7c and 8c also confirm the distinct variation in the internal features of the samples.

The dual-energy imaging provides two distinct 3D images of the plugs. The high-energy images are more sensitive to bulk density and the low-energy images are more sensitive to mineralogy. The method summarized by Wellington and Vinegar (1987) was applied on the $K_r$ sample images to compute independently the bulk density ($BD$) and the effective atomic number ($Z_{eff}$) at each CT slice position for every plug. Figure 9 shows the averaged CT-derived $BD$ and $Z_{eff}$ for the $K_r$ samples. Figure 9 also indicates reference $Z_{eff}$ values for pure calcite, dolomite and quartz (Siddiqui and Khamees, 2004). Our samples fall into two different regions on the $Z_{eff}$ axis. The good-quality RRT samples show more dolomite while the poor-quality RRT samples are mostly made of calcite. This is a fundamental difference in the mineralogy between the different RRT samples, which can have a direct effect into rock-fluid interactions and hence wettability and pore-scale fluid flow. The observations made from the CT images and dual energy data are of particular importance in such carbonate reservoirs, where dolomite-rich zones mostly have well connected intercrystalline pores, while calcite-dominated zones frequently have isolated (moldic) porosity.

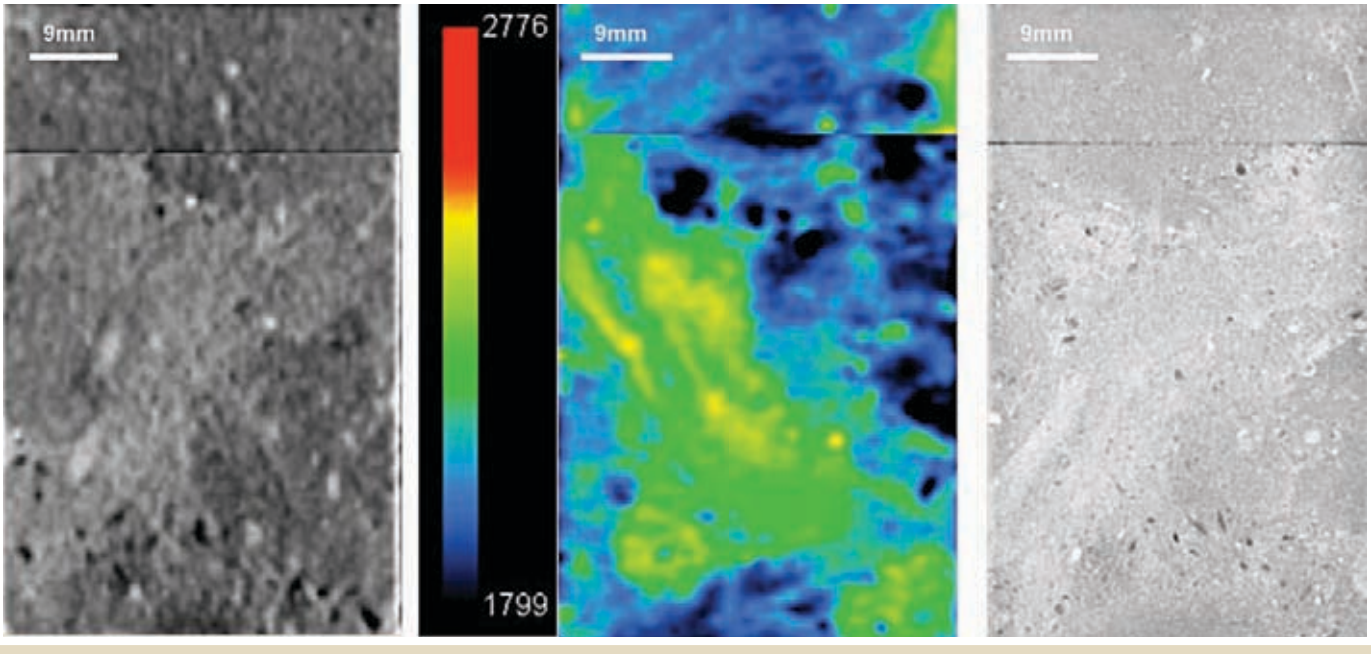


**Fig. 7**–X-ray CT-scan middle longitudinal grey-scale (left and right) and color-scale (center) images for the good-quality RRT SN-114. The plug was scanned at two resolutions: 352 μm/pixel (left and center) and 40 μm/pixel (right). The color-scale bar represents minimum and maximum pixel values in the color-scale image (center). Plug and corresponding top trim are scanned together. Direct comparison between Figs. 7 and 8 shows that the good-quality RRT sample is more heterogeneous with a high fraction of low pixels. The distribution of the low pixel space must be due to the high-permeability channel that appears as an increase in permeability over the more homogeneous SN-139. The micro-CT images in Fig. 7c (right) and Fig. 8c (right) also confirm the distinct variation in the internal features of the samples.

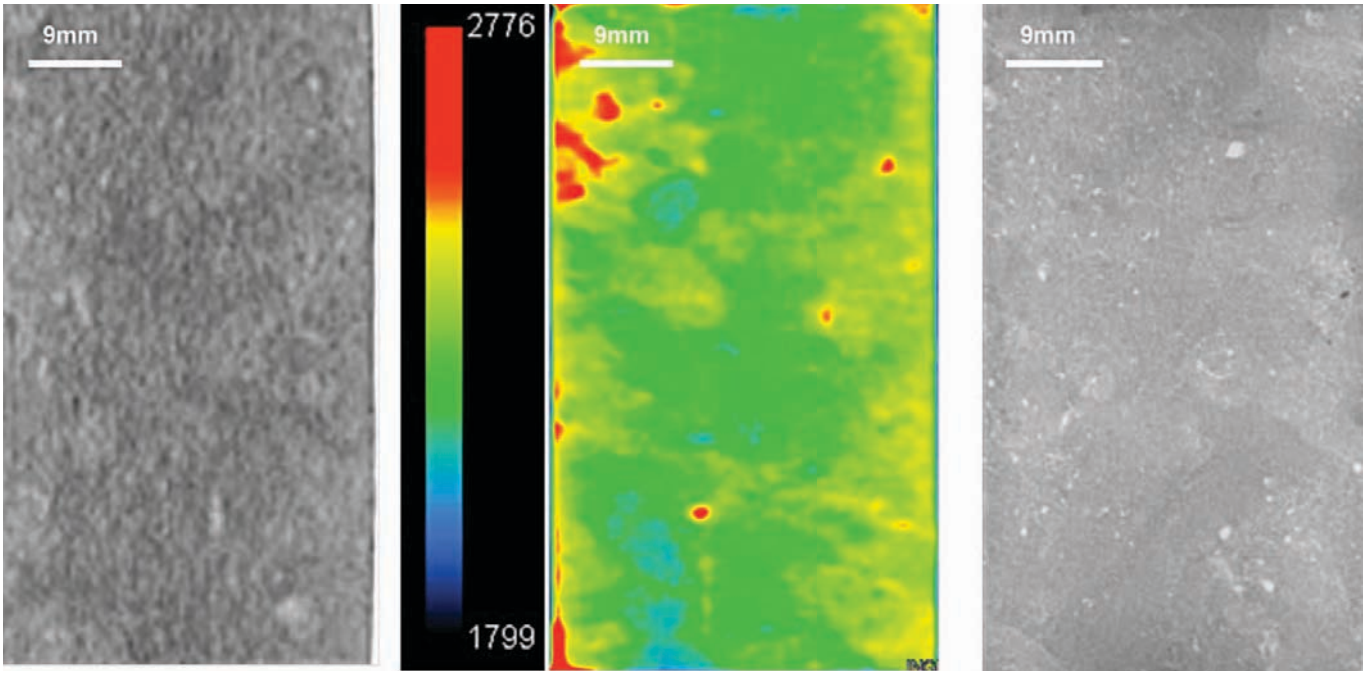


**Fig. 8**–X-ray CT-scan grey-scale (left and right) and color-scale (center) middle longitudinal images for the poor-quality RRT SN-139. The plug was scanned at two resolutions: 352 µm/pixel (left and center) and 40 µm/pixel (right). The color-scale bar represents minimum and maximum pixel values in the color-scale image (center).

Figure 9a plots the CT-derived Zeff versus grain density (GD) of the samples. The grain-density values were measured independently in the laboratory. The plot gives consistent variation in Zeff and GD for the different RRT samples, and confirms the obtained Zeff values from the dual-energy CT scanning technique. The Zeff values are very sensitive to mineralogy changes and thus were able to capture the minor grain-density variation for the good-quality RRT samples.

## Capillary Pressure and Resistivity Index

Primary drainage and imbibition experiments were performed to investigate hysteresis. All samples were thoroughly cleaned by flow-through techniques using repeated cycles of several hot solvents to render the rocks water wet (presumed wettability condition before oil entered the reservoir). The samples were then saturated with 100% simulated formation water that is assumed

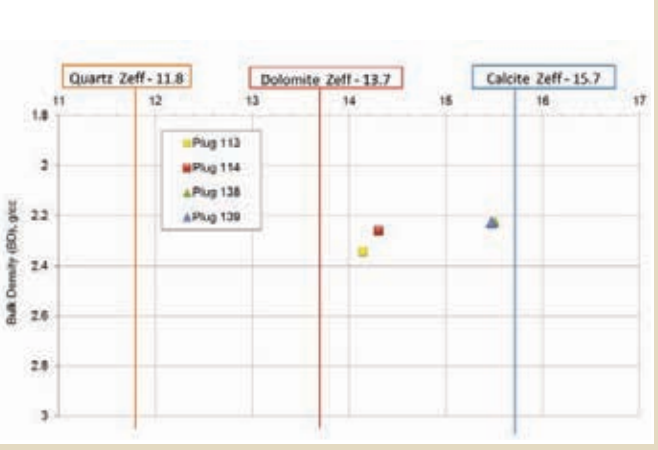


**Fig. 9**–$Z_{eff}$ versus *BD* for the $K_r$ samples. $Z_{eff}$ values are indicated for pure calcite, dolomite and quartz. The CT-derived $Z_{eff}$ values for the $K_r$ samples show that the poor-quality RRT samples are mostly calcitic while the good-quality RRT samples are more dolomitic.

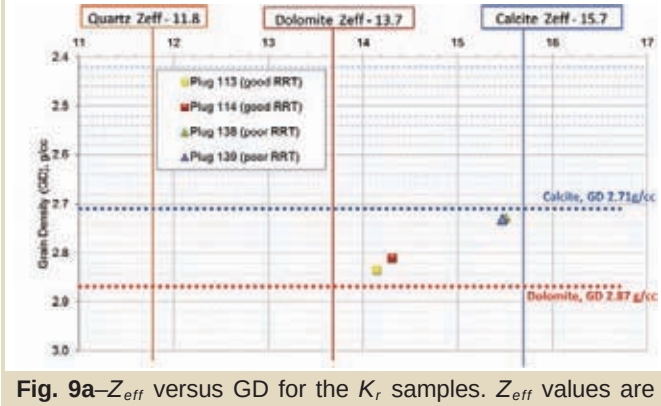


**Fig. 9a**–$Z_{eff}$ versus GD for the $K_r$ samples. $Z_{eff}$ values are indicated for pure calcite, dolomite and quartz. GD values are indicated for pure calcite and dolomite. The CT-derived $Z_{eff}$ values for the $K_r$ samples show that the poor-quality RRT samples are mostly calcitic while the good-quality RRT samples are more dolomitic. The laboratory measured GD values confirm the CT-derived $Z_{eff}$ values and the mineralogy of the samples.

**Table 1**–Flooding Rate and Capillary Number in $K_r$ Experiments

| | Good-Quality RRT | Poor-Quality RRT |
|---|---|---|
| Total flooding rate (ml/hr) | 30 | 20 |
| Capillary number ($N_c = \mu v/\sigma$) | $6.8 \times 10^{-8}$ | $4.7 \times 10^{-8}$ |

to be representative to the reservoir water composition. The capillary-pressure and resistivity-index tests were conducted by the porous-plate method at net overburden stress and reservoir temperature using dead crude oil and simulated formation brine. During primary drainage crude oil entered the rock samples at reservoir temperature. In this regard, aging would start as the oil penetrates the pore space. Eight equilibrium capillary-pressure steps were used in each saturation cycle, where the equilibrium criteria were no changes in saturation and resistivity at each step for at least seven days (total duration at each $P_c$ step was a minimum of 20 days). At the initial water saturation ($S_{wi}$) at the highest drainage $P_c$ aging continued for one month.

### Relative Permeability

The $K_r$ tests were performed at full reservoir conditions using live fluids with in-situ saturation monitoring (ISSM). All the $K_r$ samples underwent an aging period of four weeks at the end of primary drainage at full reservoir conditions without changing the experimental setup. Table 1 gives flooding rates and capillary numbers for the good-quality and poor-quality RRT samples in the relative-permeability experiments. The capillary number is given as viscous forces to capillary forces ($N_c = \mu v/\sigma$),
*where*
$\mu$ is viscosity,
$\sigma$ is interfacial tension, and
$v$ is fluid velocity.

The same flow rates were used in drainage and imbibition and the capillary numbers were comparable in both saturation cycles for each RRT. The capillary numbers provided in Table 1 are calculated from the imbibition experiments.

## EXPERIMENTAL RESULTS AND DISCUSSIONS

### Rock Typing

The relative-permeability samples are clearly distinguished by petrophyical properties and geological description. They have also been distinguished by the CT images and the CT-derived effective atomic numbers (i.e. mineralogy). Figures 3 and 4 show distinct poroperm data and PSD curves, respectively. Plugs SN-113 and SN-114 are classified as good-quality rock-type samples with higher poroperm data (21 to 46 md) and larger mean pore-throat radii (1.5 to 2.5 μm) as compared to the poor-quality rock-type samples (i.e. SN-138 and SN-139) with lower poroperm data (1 md) and smaller mean pore-throat radii (0.45 μm). Figures 5 and 6 present the thin-section photomicrographs for the good-quality RRT and poor-quality RRT samples, respectively. These figures show clear distinction between the two rock types and confirm the variations seen in poroperm and PSD. One can easily confirm the great degree of similarity between plug SN-138 and SN-139 from the petrophysical properties and indeed thin-section photomicrographs. On the other hand, plug SN-113, which gives higher permeability value than plug SN-114, shows a larger range of pore-throat radii and indeed larger pore space, as revealed by the blue colored space in the thin sections. The petrophysical property variation within the same good-quality RRT at the macroscopic scale has been supported and explained by the thin sections at the microscopic level. Geological description of the thin sections reveals that the good-quality RRT samples are characterized by fine- to medium-crystalline dolomite with a nonplanar to planar-s texture. Calcite allochems and ghost-structures of dolomitized orbitolinids, echinoderm fragments and indeterminate shell debris appear to occur locally. In addition, the pore system is dominated by common vugs and intercrystalline meso- to macropores within the locally loosely packed texture. On the other hand, the poor-quality RRT samples represent a pore system characterized by intercrystalline microporosity between microcrystalline-calcite cements and common dolomite rhombs and additional intraparticle micropores hosted in micritized grains and micritic envelopes. Interparticle pore space is reduced by micritic matrix and pore-filling calcite and dolomite cements. The CT-derived effective atomic numbers for both RRT samples are consistent with the geological description and confirm the variation in mineralogy in the rock types.

This coherent and consistent set of petrophysical data and geological description gives great confidence in the static rock-typing scheme. It would certainly be interesting to examine the effect of this static rock characterization on the dynamic data (i.e. imbibition $P_c$ and $K_r$) including hysteresis, and to test the validity of the static rock typing scheme in imbibition for an ultimate dynamic reservoir modeling (Maselmeh and Jing, 2007).

The capillary pressure and resistivity index samples range from poor-quality RRT to intermediate RRT where

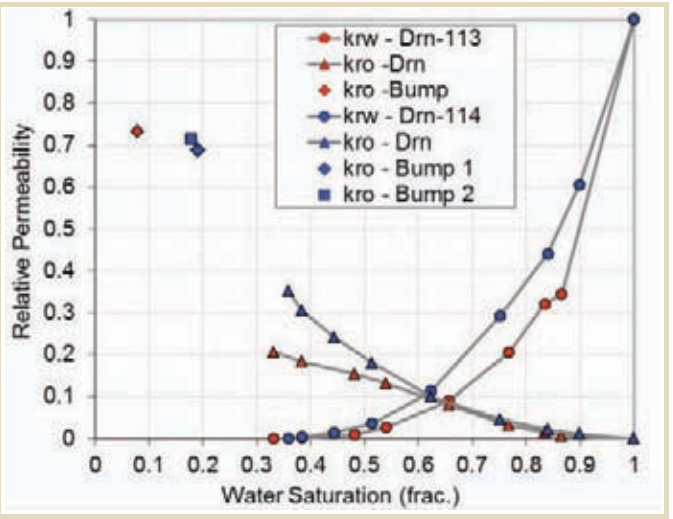


**Fig. 10**–PD $K_r$ for the good-quality RRT (two samples).

the permeability ranges from approximately 1 to 10 md, and the mean pore-throat radii vary from 0.45 to < 1 μm.

## Relative Permeability

Figure 10 shows the primary drainage (PD) relative permeability to water ($K_{rw}$) and to oil ($K_{ro}$) for the two high perm samples. These two samples (SN-113 and SN-114) represent the good-quality rock type in the reservoir. The curves show differences in the $K_r$ behavior, which can be attributed to sample heterogeneity, and which may be inferred from the CT images, poroperm data, PSD and thin-section photomicrographs. Moreover, SN-113 shows a more vuggy nature and a higher dolomite content (Fig. 9) than SN-114. Sample SN-113 suffered from capillary end effect, which caused the $K_{ro}$ curve to flatten at lower water saturation ($S_w$). A bump flood was designed to establish a more uniform $S_w$ and to reach representative initial water saturation ($S_{wi}$). The bump floods for both samples and the saturation profiles were monitored through ISSM curves along the lengths of the samples (Figs. 11 and 12). These figures present water-saturation profiles along sample length. Each profile represents equilibrium water saturation at the end of each fractional flow rate that was used during the steady-state relative-permeability experiment.

Figure 10 shows a large difference in $S_{wi}$ between the primary drainage and the bump-flood-derived values for each plug sample. The large difference in $S_{wi}$ is due to the significant capillary end effect, which is basically the saturation gradient detected in Figs. 11 and 12. The capillary end effect is defined as the accumulation of a preferentially wetting phase (i.e. water) at the outlet when displacing the wetting phase by the nonwetting phase (i.e. oil). This observation confirms that the primary drainage experiment was conducted at a preferentially water-wet condition. This, in turn, suggests that the solvent-cleaning procedures implemented at the restoration stage of the samples were efficient.

Plug SN-113 gave a lower $S_{wi}$ upon the bump flood than plug SN-114. This was expected from the pore-throat size distribution curves in Fig. 4, where plug SN-113 is at a larger pore-throat radius range compared to plug SN-114. The bump-flood rates were used to reach target $S_{wi}$ and to establish more uniform water-saturation profiles that are essential for imbibition multiphase flow experiments.

Primary drainage $K_{rw}$ and $K_{ro}$ for the low-permeability samples are plotted in Fig. 13. Both samples (SN-138 and SN-139) represent the poor-quality rock type in the reservoir and show very similar primary drainage $K_r$ characteristics. This is consistent with the CT images, and the poroperm and PSD reported earlier in Figs. 3 and 4, respectively. Their ISSM curves are given in Figs. 14 and 15, which show smoother curves compared to the curves for the high-permeability samples. One can deduce from the primary drainage $K_r$ characteristics (i.e. $K_r$ end points and $K_{rw}$-$K_{ro}$ intersections) for

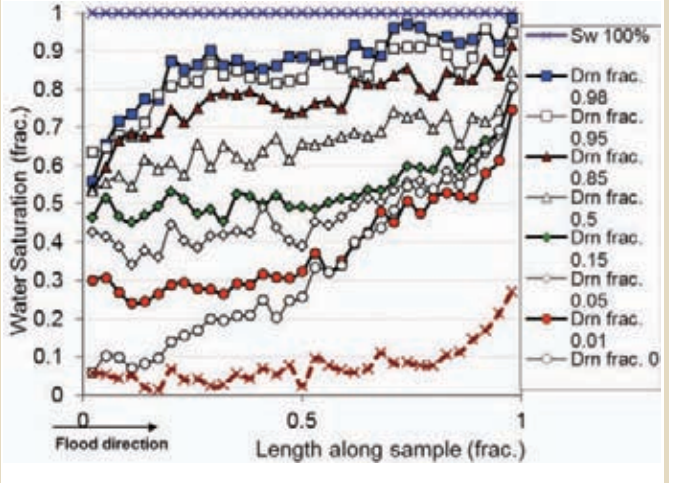


**Fig. 11**–PD ISSM curves for SN-113 (good-quality RRT). Each curve represents the Sw profile at each frac flow rate.

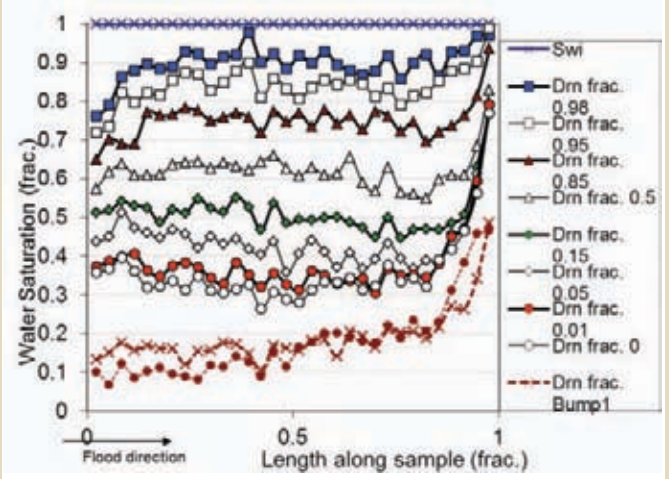


**Fig. 12**–PD ISSM curves for SN-114 (good-quality RRT). Each curve represents the Sw profile at each frac flow rate.

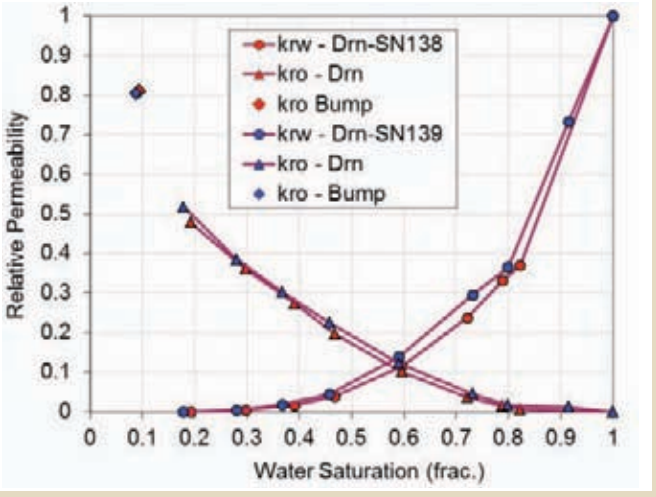


**Fig. 13**–PD $K_r$ for the poor-quality RRT (two samples).

both rock types that the samples have shown fairly water-wet behavior (Maselmeh, 2001).

Figures 16 and 17 present the imbibition relative permeability for the good-quality and the poor-quality rock types, respectively. Figure 5 gives thin-section images for samples SN-113 and SN-114 that provide more insight into the small microscale variations within the heterogeneous good-quality rock type samples. Figure 6 shows thin-section images for samples SN-138 and SN-139, which confirm the similarities between the poor-quality rock-type samples.

In Fig. 16, sample SN-114 shows more oil wet $K_r$ characteristics than sample SN-113 although both samples have similar mineralogy (i.e. mainly dolomite) and underwent similar experimental conditions. For sample SN-114 the $K_{rw}$-$K_{ro}$ intersection occurs at lower $S_w$, and the $K_{rw}$ endpoint at residual-oil saturation $K_{rw}(S_{or})$ increases to a higher level than $K_{rw}(S_{or})$ from sample SN-113. We believe the variations in imbibition $K_r$ curves are the result of the variations in drainage $K_r$ and hence the variations in the sample properties. In fact, sample SN-113 would normally be expected to show more oil wet $K_r$ characteristics since it reached lower $S_{wi}$ (Jadhunandan and Morrow, 1995) but this is not the case. We believe the $K_r$ curve is not only affected by wettability but also influenced by rock type (e.g. vugs and heterogeneity).

Figure 17 depicts the imbibition $K_r$ curves from the poor-quality RRT samples. There is very close similarity in the $K_r$ behavior between sample SN-138 and sample SN-139. This similarity must be due to the very similar basic data obtained from both samples such as porosity, permeability, pore-throat-size distribution as well as the similarity seen in the thin sections. The high degree of similarity in these basic rock properties may indicate that these two samples have similar pore geometries, which have a direct effect on the relative-permeability behavior as well as capillary pressure. It is not always possible to detect pore geometry from rock properties because there are many rock properties that can influence pore geometry. Such properties are geologically interrelated and show large variability. Therefore, it is risky to deduce the pore geometry by only looking into few of these rock properties. The variation of these properties and their effects on macroscopic properties can be evaluated and perhaps predicted if the reservoir rock is examined at the pore level.

The poor-quality samples (i.e. SN-138 and SN-139) show fewer oil-wet characteristics than the good-quality RRT samples although all plugs were treated in the same fluid pair and measured at the same experimental conditions. Before imbibition both samples were drained to low $S_{wi}$ and were aged for four weeks. So, are these samples really less oil-wet than the good-quality RRT samples? Such a conclusion may not easily be made and one should be careful when deducing wettability from macroscale property measurements. In addition to the effect of wettability, different rock types should be recognized when judging the rock behavior. Pores and/or throats will remain water wet until the surface is coated

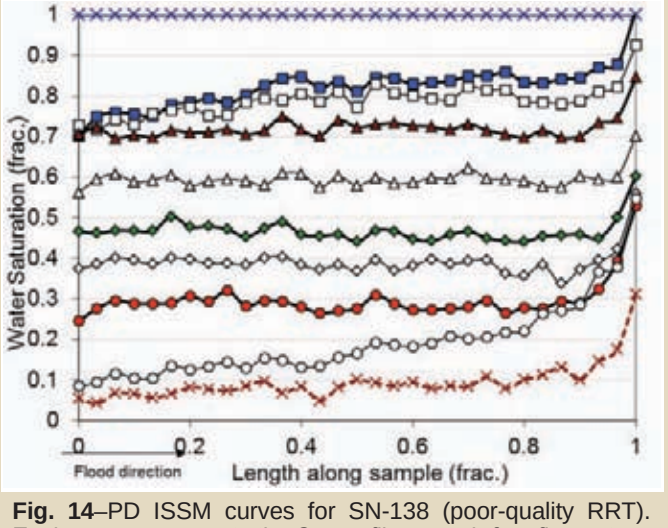


**Fig. 14**–PD ISSM curves for SN-138 (poor-quality RRT). Each curve represents the Sw profile at each frac flow rate.

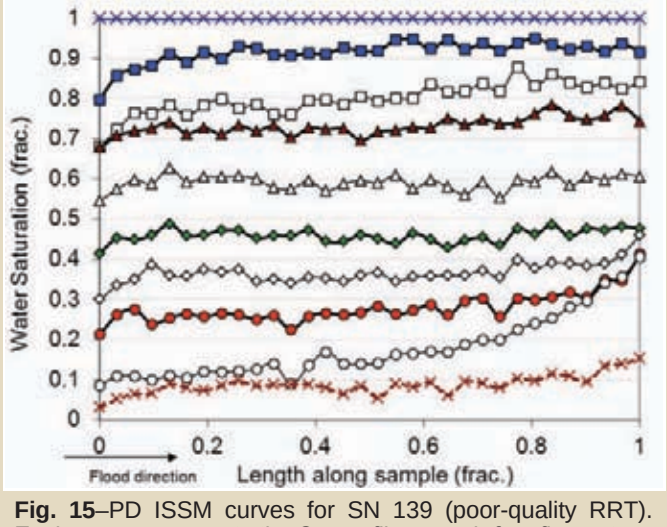


**Fig. 15**–PD ISSM curves for SN 139 (poor-quality RRT). Each curve represents the Sw profile at each frac flow rate.

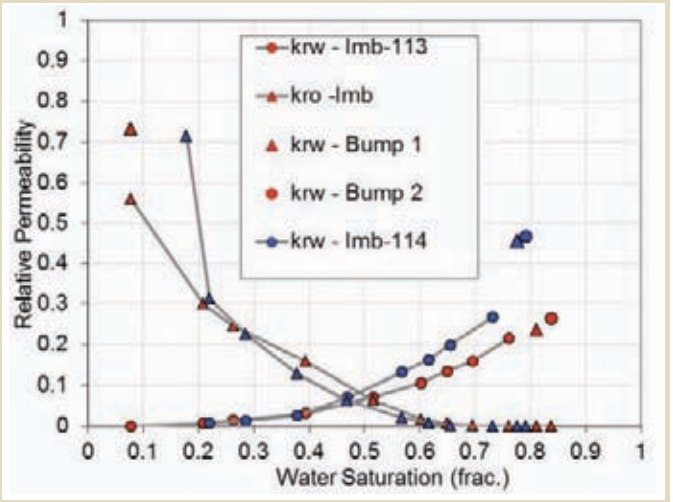


**Fig. 16**–Imb $K_r$ for the good-quality RRT (two samples).

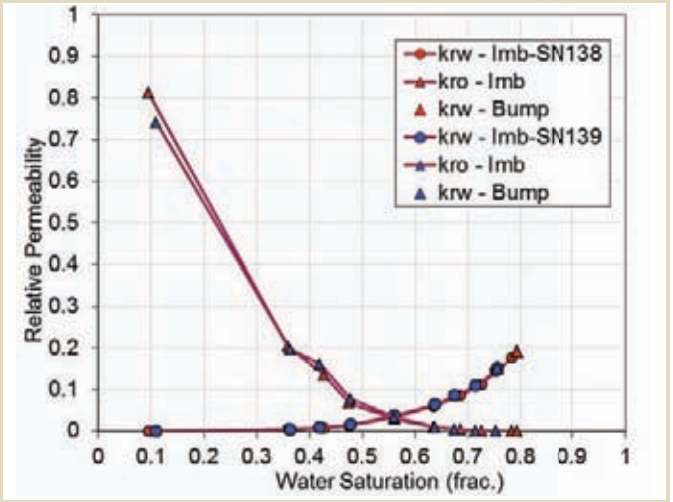


**Fig. 17**–Imb $K_r$ for the poor-quality RRT (two samples).

with an organic residue. Hence, uninvaded pore-throats and pores are generally water wet. Furthermore, oil wetting may be local, at the positive asperities in pore fabrics (e.g. pore throats or the apices of pore-wall irregularities), where water films are thinnest during primary drainage. Therefore, different rock types with various pore types may yield differences in wettability conditions at the pore scale.

The good-quality RRT samples SN-113 and SN-114 have mean pore throat radii at 2.5 and 1.5 μm, respectively, whereas the poor-quality RRT samples have mean pore radius around 0.45 μm. Such differences in pore-throat sizes, pore-throat-size distributions, possible mineralogy variation (detected from thin-section description and dual energy CT scanning) and differences in pore sizes and shapes between the different rock types can yield different wettability distributions and varying displacement mechanisms at the pore scale. It should also be mentioned here that the effect of wettability on the relative permeability endpoints is still subject for discussions, and the rules of thumb (Table 2) presented in several books (e.g. Honarpour et al., 1987) are questioned by several researchers (e.g. Morrow, 1990), especially for mixed-wettability systems.

## Relative-Permeability Hysteresis

Figure 18 plots the primary drainage and imbibition relative-permeability data for sample SN-114 from the good-quality RRT. Figure 19 plots the same type of data for sample SN-139 from the poor-quality RRT. The other samples from the given Rock types show similar hysteresis trends. Both of these figures represent relative-permeability hysteresis which can be compared with the depicted hysteresis model in Figs. 1 and 2. With direct comparison of the experimental data in both Figs. 18 and 19 to the schematic curves in Figs. 1 and 2, one can easily tell that the hysteresis model would classify the good-quality RRT samples as mixed wet

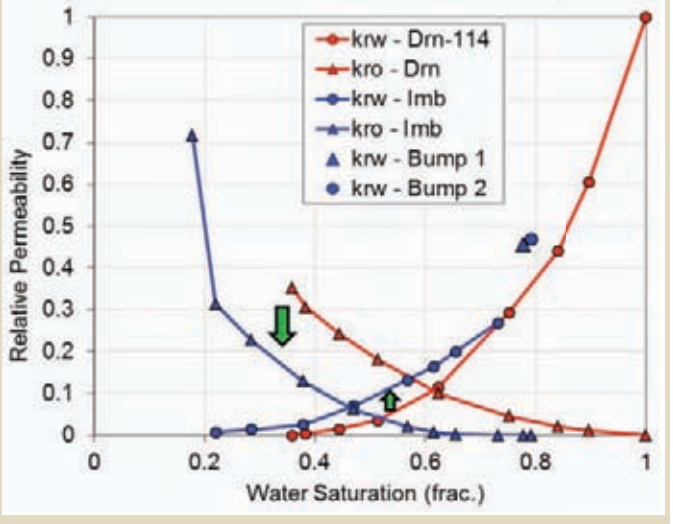


**Fig. 18**–$K_r$ hysteresis in good-quality RRT plug SN-114. Green arrows indicate direction of hysteresis.

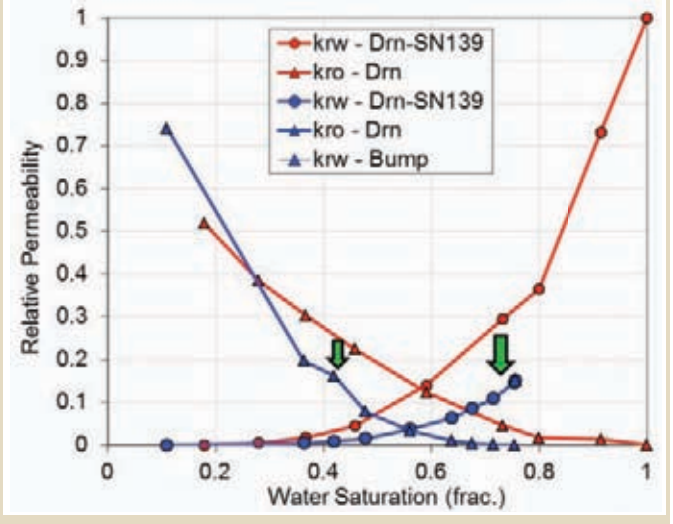


**Fig. 19**–$K_r$ hysteresis in poor-quality RRT plug SN-139. Green arrows indicate direction of hysteresis.

**Table 2**–Rules of Thumb for the Effect of Wettability on $K_r$ Endpoints (Honapour et al., 1987)

| | Water-wet | Oil-wet |
|---|---|---|
| Irreducible $S_w$ | > 20-25% | < 15% |
| $S_w$ at which $K_{ro} = K_{rw}$ | > 50% | < 50% |
| $K_{rw}(S_{or})/K_{ro}(S_{wi})$ | < 0.30 | > 0.50 |

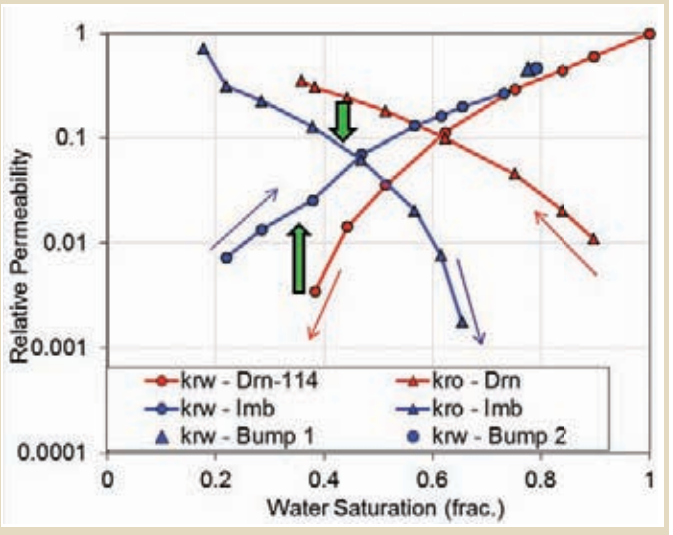


**Fig. 20**–Semilog representation of Fig. 18. Red and blue arrows indicate direction of $K_r$.

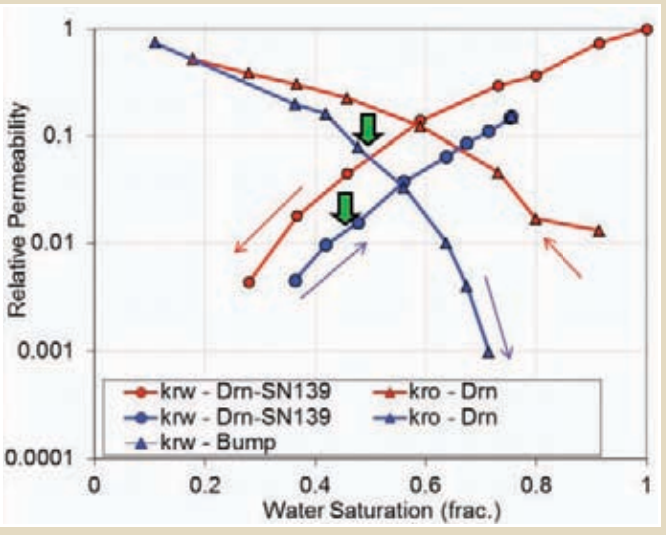


**Fig. 21**–Semilog representation of Fig. 19. Red and blue arrows indicate direction of Kr.

and the poor-quality RRT samples as water wet. Figures 20 and 21 present the hysteresis trends in semilog axes to emphasize the strong experimental hysteresis measured in these rock types.

For the good-quality RRT samples the possible pore-level scenario could be that all pores were converted to oil wet at the end of drainage (after aging). This will be later emphasized by spontaneous imbibition behavior from the $P_c$ experiments. At the start of imbibition, water invades the largest pores first giving rise to higher imbibition $K_{rw}$ than drainage $K_{rw}$. In drainage water was moving in smaller pores at a given $S_w$. The flow mechanism in this imbibition process is mainly piston-like displacement with less oil trapping (Lenormand et al., 1983). This is also evidenced by the approach of the imbibition $K_{rw}$ curve to the drainage $K_{rw}$ curve (see semilog Fig. 20). Imbibition $K_{ro}$, on the other hand, moves downward as compared to drainage $K_{ro}$ since less oil is left in the large pores during imbibition (Maselmeh, 2001). This explanation of the oil-wet case apparently does not apply to the poor-quality RRT samples. For this RRT the possible scenario could be that fewer pores were converted to oil wet. Hence, oil trapping is pronounced during imbibition by possible snap-off mechanism (Lenormand et al., 1983). This oil trapping will cause lower mobile oil saturation and hence will shift both imbibition $K_{ro}$ and $K_{rw}$ to the left (see Fig. 1). At the same time, the oil trapped in the middle of the pores may hinder water flow and thus may lower imbibition $K_{rw}$ below drainage $K_{rw}$. So, imbibition $K_{rw}$ may have opposing factors in the hysteresis behavior. If the opposing factors are equal we may end up with no hysteresis in $K_{rw}$ (Maselmeh, 2001). This explanation is consistent with earlier investigations, which observed that in almost all capillary-dominated flows of strongly wetting phases, the nonwetting phase $K_r$ showed much more hysteresis than the wetting phase (Jerauld and Salter, 1990). The experimental hysteresis results from our poor-quality RRT samples may suggest that the oil trapping effect is the dominating factor and must be mainly governed by the geometric and topologic properties of the pore space. These properties are related to pore-throat-size ratio, type and extent of heterogeneity, throat-to-pore coordination number and surface condition of the pores. In strongly water-wet systems these geometric properties are of first-order importance in controlling trapping. In less water-wet systems the pore geometry becomes less significant (Wardlaw, 1980), and this suggests combined wettability and pore-geometry effects in yielding the different hysteresis trends observed in the different rock types under this research study.

It is interesting to see only minor differences (Fig. 22) in the shapes of the primary drainage relative-permeability curves between sample SN-114 from the good-quality RRT and sample SN-139 from the poor-quality RRT. In the imbibition mode (Fig. 23) there is a profound difference in the relative-permeability behavior between the same samples. This behavior can be attributed to the interaction effect between wettability and rock type (i.e. pore space) on

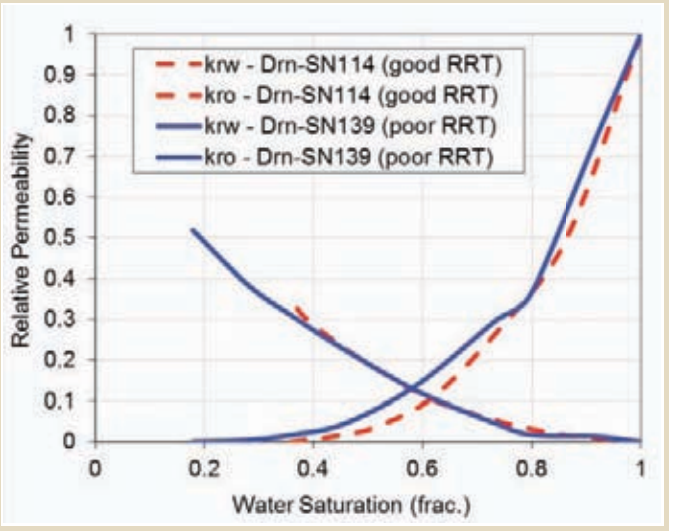


**Fig. 22**–Comparison of drainage $K_r$ between RRTs.

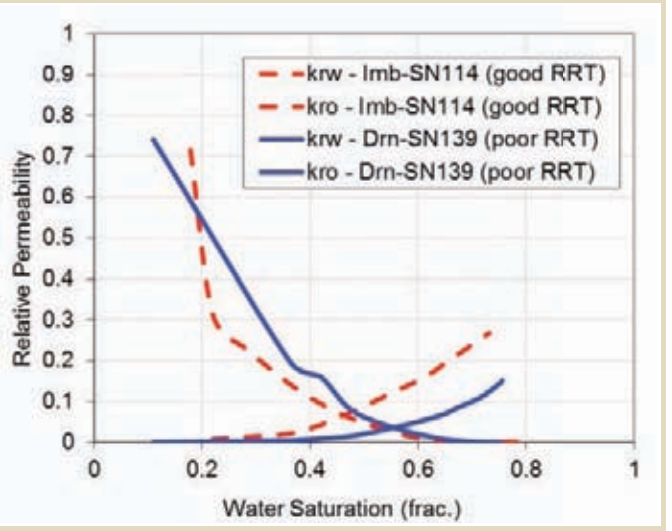


**Fig. 23**–Comparison of imbibition $K_r$ between RRTs.

the complex displacement mechanisms involved in the imbibition process.

Figure 22 does not show the data acquired after the bump floods. Lower $S_{wi}$ was obtained for the poor-quality RRT sample (i.e. 0.179 frac) as compared to the good-quality RRT sample (i.e. 0.359 frac). One would assume higher permeability samples to yield lower $S_{wi}$ values. This is apparently not always the case if we have vuggy and heterogeneous systems like the good-quality RRT sample in this study. Heterogeneity can be identified by the specific types and relative percentages of pores present, and their distribution within a porous medium. The good-quality RRT sample is characterized by vugs, and has wider range of pore-throat radii. Such a system can promote water trapping during oil injection, especially towards the outlet end of the plug sample. In such a porous system, in primary drainage, the preference of oil flow would be the large pores and connected vugs. Smaller water-filled pores may get bypassed by the overall large channels in the sample. The smaller pores are only partially swept by oil due to pressure gradient along the sample length. In less heterogeneous samples (like the poor-quality RRT sample) with uniform pore-throat-size distributions large flow channels are absent and hence less chance of the water-trapping effect.

## Capillary Pressure and Resistivity Index

Experiments were performed by the porous-plate method, which allows for combined capillary-pressure and resistivity-index (*PcRI*) measurements. Figure 24 shows the primary drainage and imbibition capillary-pressure curves for the samples whose poroperm data and PSD curves were given in Figs. 3 and 4, respectively. The samples spent over 12 months in the drainage cycle with crude oil at reservoir temperature. This experimental condition is expected to yield nonwater-wet state at the end of drainage, which was confirmed by the absence of spontaneous imbibition upon stepwise decrease of $P_c$ level to zero. Forced imbibition curves declined to low residual-oil saturations $S_{or}$ (i.e. $S_w \sim 0.8$ to 0.9), which is another indication of mixed-wet to oil-wet condition where water can invade in piston-like displacement mechanism and oil production is possible through oil films (Salathiel, 1973).

Figure 25 depicts one sample example for drainage and imbibition resistivity-index data as a function of water saturation. Figures 26 and 27 present all sample *RI* curves for drainage and imbibition, respectively. There is clear hysteresis in *RI* between drainage and imbibition cycles causing hysteresis in the calculated Archie saturation exponent *n* as well.

Hysteresis in resistivity can be explained by a proposed water-invasion mechanism at the pore level. At the end of drainage almost all invaded pores are oil wet (absence of spontaneous imbibition). Initial water saturation ($S_{wi}$)

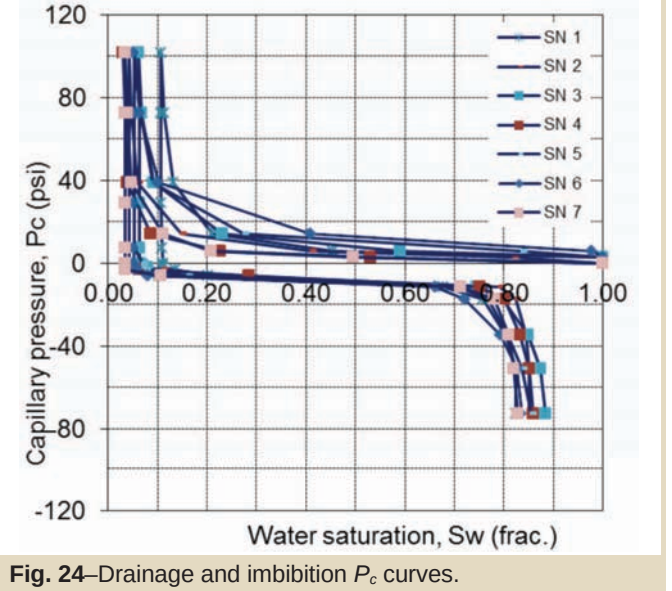


**Fig. 24**–Drainage and imbibition $P_c$ curves.

accounts for bulk water in noninvaded small pores, bulk water in the surface grooves, nooks and crannies of the pore walls and small fraction of adsorbed water films, which probably account for less than one saturation percent (Morrow, 1970; Jerauld and Salter, 1990). Electric conductivity is only possible through water present in the noninvaded pores and in pore-wall grooves. Adsorbed-water films must have been replaced by oil films as part of conversion to oil wetness during primary drainage (Kaminsky and Radke, 1997). Water in the pores and pore-wall grooves may not totally participate in the electric conductivity unless it is all in hydraulic conductivity (Gladkikh and Bryant, 2005). As imbibition starts with low negative $P_c$ water invades largest pores only. Capillary pressure is fixed at the low level until water invasion (i.e. oil production) ceases as part of the porous-plate experimental design. Resistivity starts dropping as water invasion proceeds. Water at this stage does not invade all pores, and thus water does not span the porous medium especially if the large pores are fewer in number and not well connected. The invading water may not come to a complete connectivity with the existing water at $S_{wi}$. Hence, resistivity does not drop enough to equate the effect of increasing $S_w$ in the Archie equation, hence saturation exponent $n$ is higher than that of drainage at the same $S_w$. As water invades smaller pores at increasing negative $P_c$ levels water starts connecting and an increasing drop in resistivity occurs until it approaches the drainage *RI* curve. This behavior is clearly seen (in all the samples) which suggests imbibition takes place through piston-like displacement with less oil trapping.

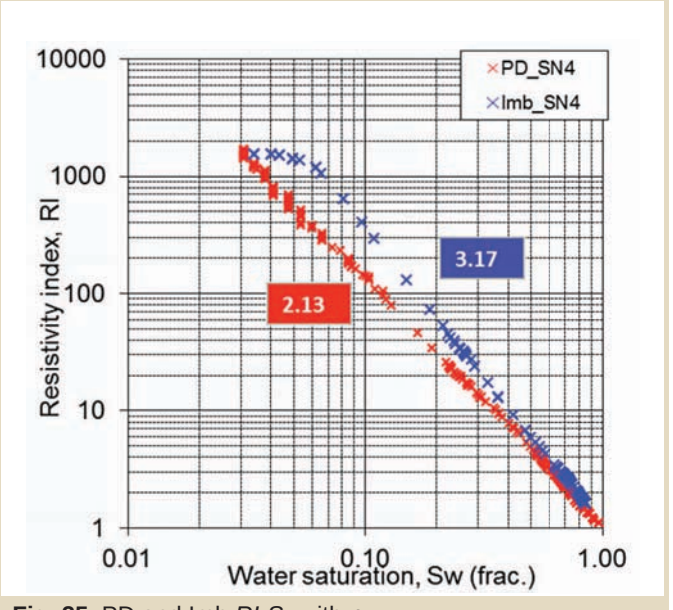


**Fig. 25**–PD and Imb *RI*-$S_w$ with *n*.

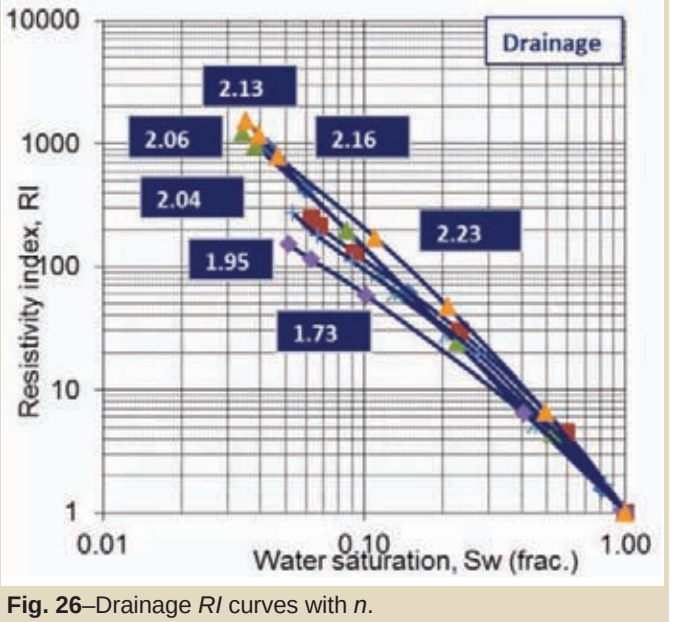


**Fig. 26**–Drainage *RI* curves with *n*.

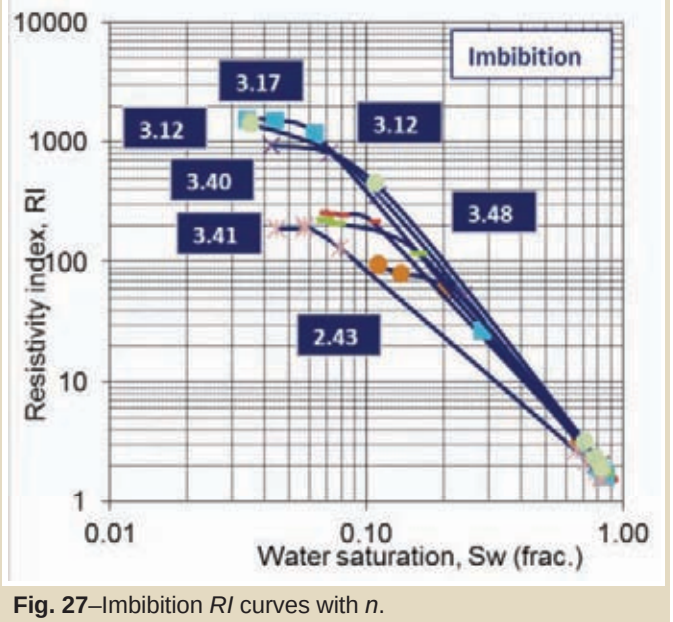


**Fig. 27**–Imbibition *RI* curves with *n*.

## CONCLUSIONS AND OBSERVATIONS

1. High-permeability good-quality rock-type samples showed a higher tendency towards oil-wet relative-permeability behavior compared to the poor-quality rock-type samples. This is also confirmed from previous wettability indices on similar rock types.
2. Primary-drainage and imbibition relative-permeability curves showed different hysteresis patterns on different rock type samples, which could be attributed to the combined effect of wettability and pore geometry.
3. The initially established static rock-typing scheme based on petrophysical properties and geological description was validated by imbibition relative-permeability and hysteresis trends. This validation is essential when assigning saturation functions into dynamic reservoir modeling.

4. CT-derived effective atomic number on the whole-core plugs confirmed the variations in mineralogy between different rock types. This could have a direct effect on wettability, and hence on pore-scale multiphase flow.

5. Strong hysteresis in *RI* and *n* was explained by a proposed fluid-invasion behavior at the pore level, and is attributed to varying displacement mechanisms between primary drainage and imbibition. Conventional assumption of Archie behavior is therefore not always valid for such carbonate rock types.

6. Our results suggest significant impact on the estimations of remaining oil saturation, and hence proper hysteresis measurements are important for better quantification of hydrocarbon recovery and trapped fluid saturations.

7. The experiments in this study show that hysteresis effects in general cannot be neglected, but for practical applications it may suffice to extend the measured data range by correlations, numerical network models and/or digital rock physics.

## NOMENCLATURE

### Symbols

| | |
|---|---|
| *BD* | Bulk Density |
| *GD* | Grain Density |
| σ | Interfacial Tension |
| $K_L$ | Klinkenburg Corrected Gas Permeability |
| $K_r$ | Relative Permeability |
| $K_{ro}$ | Oil Relative Permeability |
| $K_{rw}$ | Water Relative Permeability |
| *n* | Archie Saturation Exponent |
| $N_c$ | Capillary Number |
| $P_c$ | Capillary Pressure |
| *RI* | Resistivity Index |
| $S_w$ | Water Saturation |
| $S_{wi}$ | Initial Water Saturation |
| $S_{or}$ | Residual Oil Saturation |
| *v* | Velocity |
| μ | Viscosity |
| $Z_{eff}$ | Effective Atomic Number |

### Abbreviations

| | |
|---|---|
| Frac | Fractional |
| Imb | Imbibition |
| ISSM | In-Situ Saturation Monitoring |
| *PcRI* | Capillary Pressure and Resistivity Index |
| PD | Primary Drainage |
| PSD | Mercury-Derived Pore Throat Size Distribution |
| RRT | Reservoir Rock Type |
| SN | Sample Number |

## ACKNOWLEDGEMENTS

The authors wish to acknowledge ADNOC and ADCO Management for permission to publish the results of this SCAL study entailed in this paper. Ingrain Inc.-Abu Dhabi are acknowledged for providing the dual-energy CT scanning and plug micro-CT images. The authors also wish to thank Ahmed Dawoud for his contribution to the work, and the primary author is grateful to Ove Bjorn Wilson for his review and useful comments on the paper.

## REFERENCES

Anderson, W.G., 1987a, Wettability Literature Survey – Part 4: Effects of Wettability on Capillary Pressure, Paper SPE-15271, *Journal of Petroleum Technology*, **39**(10), 1283-1300.

Anderson, W.G., 1987b, Wettability Literature Survey – Part 5: The Effects of Wettability on Relative Permeability, Paper SPE-16323, *Journal of Petroleum Technology*, **39**(11), 1453-68.

Dernaika, M., Efnik, M.S., Koronful, M.S., Al Mansoori, M., Hafez, H., and Kalam, M.Z., 2007, Case Study for Representative Water Saturation from Laboratory to Logs and the Effect of Pore Geometry on Capillarity, Paper SCA2007-38 presented at the International Symposium of the Society of Core Analysts, Calgary, Canada, 18-21 September.

Fleury, M., Efnik, M.S., and Kalam, M.Z., 2004, Evaluation of Water saturation from Resistivity in a Carbonate Field, Paper SCA 2004–22, presented at the International Symposium of the Society of Core Analysts, Abu Dhabi.

Gladkikh, M., and Bryant, S., 2005, Prediction of Imbibition in Unconsolidated Granular Materials, *Journal of Colloid and Interface Science*, **288**, 526–539.

Hirasaki, G.J., 1991, Thermodynamics of Thin Films and Three-Phase Contact Regions, in N.R. Morrow (ed.), *Interfacial Phenomena in Oil Recovery*, Marcell Dekker, New York, 23-76.

Honarpour, M., Koederitz, L., and Harvey, A.H., 1987, *Relative Permeability of Petroleum Reservoirs*, CRC Press Inc, Boca Raton.

Jadhunandan, P.P., and Morrow, N.R., 1995, Effect of Wettability on Waterflood Recovery for Crude-Oil/Brine/Rock Systems, Paper SPE-22597, *SPE Reservoir Engineering*, **10**(1), 40-46.

Jerauld, G.R., and Salter, S.J., 1990, Effect of Pore-Structure on Hysteresis in Relative Permeability and Capillary Pressure: Pore-Level Modeling, *Transport in Porous Media*, **5**, 103-151.

Kaminsky, R., and Radke, C.J., 1997, Asphaltenes, Water Films, and Wettability Reversal, Paper SPE-39087, *SPE Journal*, **2**, 485-493.

Kovscek, A.R., Wong, H., and Radke, C.J., 1993, A Pore-Level Scenario for the Development of Mixed Wettability in Oil Reservoirs, *AIChE Journal*, **39**(6), 1072–1085.

Lenormand, R., Zarcone, C., and Sarr, A., 1983, Mechanisms of the Displacement of One Fluid by Another in a Network of Capillary Ducts, *Journal of Fluid Mechanics,* **135**, 337-353.

Longeron, D.G., Argaud, M.J., and Feraud, J.-P., 1989, Effect of Overburden Pressure and the Nature and Microscopic Distribution of Fluids on Electrical Properties of Rock Samples, Paper SPE-15383, *SPE Formation Evaluation,* **4**(2), 194-202.

Longeron, D., Hammervold, W.L., and Skjaeveland, S.M., 1994,Water-Oil Capillary Pressure and Wettability Measurements Using Micropore Membrane Technique, Paper SCA 1994-26 presented at the International Symposium of the Society of Core Analysts.

Masalmeh, S.K., 2001, Experimental Measurements of Capillary Pressure and Relative Permeability Hysteresis, Paper SCA 2001-23 presented at the International Symposium of the Society of Core Analysts, Edinburgh, September.

Masalmeh, S.K., and Jing, X.D., 2006, Capillary Pressure Characteristics of Carbonate Reservoirs: Relationship Between Drainage and Imbibition Curves, Paper SCA 2006-16, presented at the International Symposium of the Society of Core Analysts, Trondheim, Norway, 12-16 September.

Masalmeh, S.K., and Jing, X.D., 2007, Improved Characterization and Modelling of Carbonate Reservoirs for Predicting Waterflooding Performance, Paper IPTC-11722, presented at the International Petroleum Technology Conference, Dubai, U.A.E., 4-6 December.

Melrose, J.C, 1965, Wettability as Related to Capillary Action in Porous Media, Paper SPE-1085, *SPE Journal,* **5**(3), 259-271.

Morrow, N.R., 1970, Irreducible Wetting-Phase Saturations in Porous Media, *Chemical Engineering Science,* **25**, 1799-1815.

Morrow, N.R., 1990, Wettability and its Effect on Oil Recovery, Paper SPE-21621, *Journal of Petroleum Technology,* **42**(12), 1476-84.

Salathiel, R.A., 1973, Oil Recovery by Surface Films Drainage in Mixed-Wettability Rocks, Paper SPE-4104, *Journal of Petroleum Technology,* **25**(10), 1216-1224.

Serag El Din, S., Dernaika, M.R., Al Hosani, I., Hannon, L., Skjæveland, S.M., and. Kalam, M.Z., 2010, Whole Core Versus Plugs: Integrating Log and Core Data to Decrease Uncertainty in Petrophysical Interpretation and STOIP Calculations, Paper SPE-137679 presented at the Abu Dhabi International Petroleum Exhibition and Conference held in Abu Dhabi, UAE, 1–4 November.

Siddiqui, S., and Khamees, A.A., 2004, Dual-Energy CT-Scanning Applications in Rock Characterization, Paper SPE-90520, presented at the SPE Annual Technical Conference and Exhibition held in Houston, Texas, U.S.A., 26-29 September.

Toledo, P.G., Scriven, L.E., and Davis, H.T., 1994, Pore-Space Statistics and Capillary Pressure Curves From Volume-Controlled Porosimetry, Paper SPE-19618, *SPE Formation Evaluation,* **9**(1), 46-54.

Wardlaw, N.C, 1980, The Effects of Pore Structure on Displacement Efficiency in Reservoir Rocks and in Glass Micromodels, Paper SPE-8843 presented at the First Joint SPE/DOE Symposium on Enhanced Oil Recovery, Tulsa, Oklahoma, 20-23 April.

Wardlaw, N.C, 1982, The Effects of Geometry, Wettability, Viscosity and Interfacial Tension on Trapping in Single Pore-Throat Pairs, Paper 82-02-01, Journal of Canadian Petroleum Technology, **21**(3).

Wellington, S.L. and Vinegar, H.J., 1987, X-Ray Computerized Tomography, Paper SPE-16983, *Journal of Petroleum Technology,* **39**(8), 885-898.

## ABOUT THE AUTHORS

**Moustafa R. Dernaika** is the Manager of Ingrain Inc. - Abu Dhabi since 2010. Before he joined Ingrain he worked for Emirates Link ResLab LLC (Weatherford Laboratories) as the Regional SCAL Manager in Abu Dhabi. He had 10 years of Routine and Special Core Analysis experience with special interest in Business Development, Project Management and Data Interpretation. Moustafa holds BS and MS degrees from the Middle East Technical University in Ankara, both in Chemical Engineering. He is currently continuing his PhD study in Petroleum Reservoir Engineering at the University of Stavanger in Norway. Moustafa's current research areas include digital rock physics and dual-energy CT applications. He also works on the variation of petrophysical measurements with rock types and wettability.

**Mohammed Zubair Kalam** is a Discipline Expert in special core analysis for Abu Dhabi Company for Onshore Oil Operations, with 25 years of petroleum industry experience. After completing his BSc and PhD degrees at the University of Manchester and post-doctoral research at the University of Oxford, he joined BP, where he was involved in novel core analysis research involving nuclear magnetic resonance and magnetic resonance imaging, as well as single-phase and multiphase fluid flow. Zubair has been recognized with the SPE 2012 Regional Technical Award in Formation Evaluation, and is actively involved in Advanced SCAL, CO2 EOR studies and Digital Rock Physics analyses in carbonates.

**Mahmoud A. Basioni** holds a master's degree in petroleum engineering from the University of Texas at Austin. He currently works as a senior reservoir engineer in ADCO where his major responsibilities are reservoir modeling and development studies. His interests are compositional modeling, SCAL, and EOR. Mr. Basioni is currently working on a development study for a major Middle East carbonate reservoir, which involves WAG injection under miscible conditions.

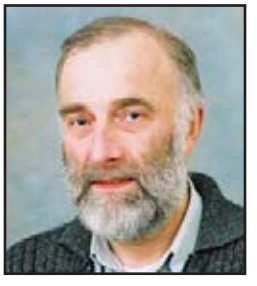

**Svein M. Skjæveland** is a Professor of Reservoir Engineering at the University of Stavanger. He holds doctorate degrees in engineering physics from the Technical University of Norway and in petroleum engineering from Texas A&M University. He was in charge of developing the MS and PhD programs in petroleum engineering in Stavanger and the petroleum engineering research branch of the International Research Institute of Stavanger. Presently he works on in-situ wettability determination by NMR and three-phase capillary pressure correlations.